Etching with an ECR Plasma

Walter J. Varhue and Andrew J. Watts

Dept. of Electrical Engineering
University of Vermont
Burlington, VT. 05405

Abstract

An electron cyclotron resonance plasma is used to etch organic resist with oxygen and Si with SF_6. Etch performance was studied as a function of operating conditions, resonance chamber geometry and composition of the microwave window. Using a quartz microwave window results in the redeposition of a thin SiO_2 layer on the Si substrate surface. This significantly impacts etch performance.

Etch rate studies performed on Si with a SF_6 plasma revealed an unexpected saturation with atomic fluorine concentration. A model based on the Cabrera-Mott mechanism is developed to explain the saturation. The rate limiting step for conditions with both high free fluorine flux and low ion energy bombardment is due to electron tunnelling from the Si bulk, through the fluorosilyl layer, to the adsorbed fluorine.

Introduction

Plasma etching with an electron cyclotron resonance(ECR) source has a number of advantages for single wafer processing of sub-micron features. The ECR generates a high density plasma (10^{12} cm^{-3}) which yields high etch rates and possibly high through-put. The discharge can and must be maintained at a low process pressure, 0.5 to 5 x 10^{-3} Torr(0.07 to 0.7 Pa). At these pressures the mean free path of plasma species is on the order of chamber dimensions (>10 cm). This permits the resonance zone to be spatially separated from the substrate. This allows a decoupling of the plasma species production occurring in the ECR zone from energetic ion bombardment of the substrate, which can be independently controlled through RF substrate biasing. Another result of the long mean free path lengths is that the plasma stream is composed of less scattered ions which arrive perpendicular to the substrate. There is no need for large substrate biases to re-direct the ion flux to obtain anisotropic etching. The lower ion energies are welcomed because of concerns raised over the effects of material damage on device performance.

The ECR process, however, is not without its problems. There are concerns with radial uniformity in the diverging downstream magnetic field. The ECR magnets are large and interference with one another may prevent the incorporation of ECR into a cluster tool configuration. The ECR process is very inefficient with most of the input power heating the resonance chamber walls. The walls are typically cooled which in practice becomes a source of particulate contamination. High energy electrons in the ECR zone produce x-rays which may electrically damage oxide materials on the substrate.[1]

In this investigation, an ECR has been used to etch multilayer resist (MLR) structures with an oxygen plasma, and silicon with a SF_6 plasma at cryogenic substrate temperatures. Specifically, some interesting effects regarding reactor geometry and microwave window composition have been observed. Further, a saturation in the etch rate of Si with SF_6 has been observed. A model has been proposed based on the Cabrera -Mott mechanism to account for the experimental observation.

Experimental

Apparatus

The etching study was performed in a custom built ECR reactor, a sketch of which is shown in Fig. 1. Microwave power at 2.45 GHz is applied to the resonance chamber through a quartz

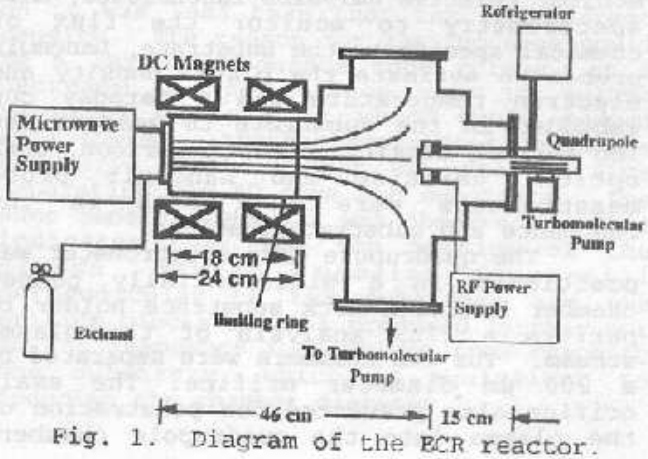

Fig. 1. Diagram of the ECR reactor.

window. The microwave applicator has a gradual transition from a WR 284 guide to an 11 cm. diameter cylindrical segment. Two electromagnets are located around the resonance chamber and provide a magnetic field of approximately 925 G near the window which drops to the required ECR condition of 875 G at approximately 5 cm into the chamber. The resonance chamber is 15.25 cm in diameter, 23 cm long and is separated from the substrate chamber by a constricting orifice that is typically 9 cm in diameter. The resonance chamber diameter was modified with two stainless steel cylindrical inserts

The substrate holder was constructed by bonding a 10 cm diameter aluminum plate to a copper coil through which a refrigerant mixture of freon and Ar was circulated. The bond was made with a stycast epoxy material with high thermal conductivity and low electrical conductivity. The chuck could be cooled to -100 °C with a Polycold chiller. Thermal contact to the samples, which were 3 cm by 3 cm squares, cut from 5 in. silicon wafers, was obtained by a thin coating of Dow Corning 704 grease. Samples were clamped into place behind a counter sunk retaining ring. The retaining ring prevented plasma exposure to the grease as well as provided a thermal break between the plasma and the chuck.

Sample Preparation and Etching

The samples to be etched contained either patterned MLR structures or blanket polysilicon on single crystal wafers. The MLR structure consisted of a 1 μm thick planarizing layer of Novolac resist, 100 nm plasma deposited silicon dioxide, and 0.8 μm of exposed and developed photoresist. The oxide layer was opened using a short fluorine based plasma etch in a standard reactive ion etch(RIE) reactor.

Diagnostics

The ECR plasma stream was characterized using standard optical emission(OES) to monitor relative emission intensities, mass spectrometry to monitor the flux of chemical species to the substrate, Langmuir probes to estimate the plasma density and electron temperature and a Faraday cup embedded in the substrate to measure the ion current density. For comparison, both optical emission and Langmuir probe measurements were made both in the resonance and substrate chambers.

The quadrupole mass spectrometer was positioned in a differentially pumped chamber behind a mock substrate holder to perform a flux analysis of the plasma stream. The two chambers were separated by a 200 μm diameter orifice. The small orifice also prevented the penetration of the plasma into the quadrupole chamber. This apparatus was used to measure of the relative magnitudes of atomic and molecular species in the oxygen plasma stream. It was also used to qualitatively identify constituents in the SF_6 plasma stream.

Discussion of Results

Etch Rate Performance

There are a number of factors which have been observed to influence etch rate performance. These are reactor geometry, magnetic field configuration, and operating parameters such as power, pressure and flow rate. These observations have been used to develop a qualitative model of the ECR process. Practically all ion and radical species production occurs in the resonance zone. The ionic and neutral species diffuse downstream toward the substrate region. The ionic species are directed by the parallel magnetic field. Both species undergo scattering collisions with gas molecules which cause them to be lost from the plasma stream. They are scattered to the chamber walls where they are lost through recombination or other chemical reactions. Consider for example, an oxygen plasma stream. As process pressure increases, so does the density of possible scattering sites along the path. A plot of the ion current density as a function of pressure is plotted in Fig. 2. The calculated scattering cross section from this curve is $\sigma = 0.12\ nm^2$. This value is in reasonable agreement with the charge exchange cross section for O_2^+ in an oxygen ambient $\sigma = 0.15\ nm^2$.[2] Similar behavior is expected for the atomic oxygen flux. A curve of the atomic oxygen flux plotted as a function of process pressure is shown in Fig. 3. The initial increase with pressure is simply due to the increased density of reactant atoms available for dissociation. One factor which can be used to increase etch rate is to reduce the distance which separates the resonance zone and the substrate.

As stated earlier the vast majority of ion and radical species production is expected to occur in the resonance zone. The resonance zone contains a high density of electrons whose energy distribution is assumed to be Maxwellian. A reactant molecule entering this region is likely to undergo dissociation because of the large

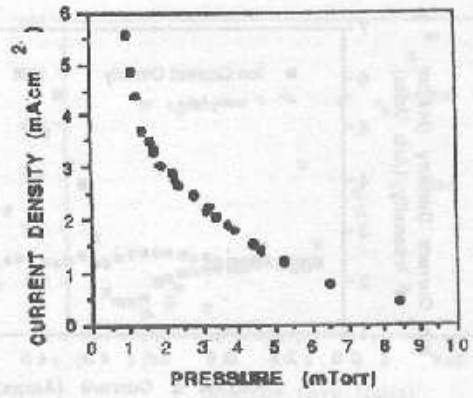

Figure 2. Ion current density in an oxygen plasma as a function of process pressure.

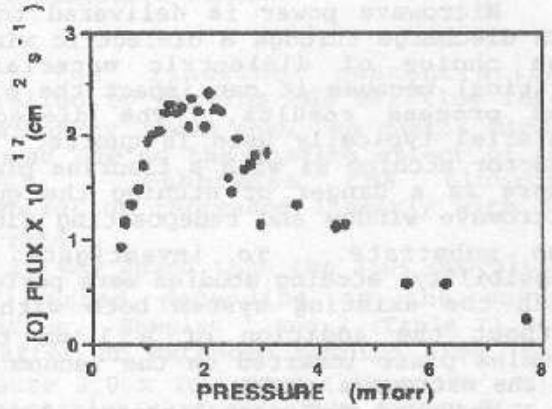

Figure 3. Oxygen flux density as a function of reactor pressure.

density of low energy electrons. This behavior is exhibited in Fig. 4 where free fluorine concentration in an SF_6 discharge is plotted as a function of microwave power for three different flow rates. The cross section for electron collisions leading to

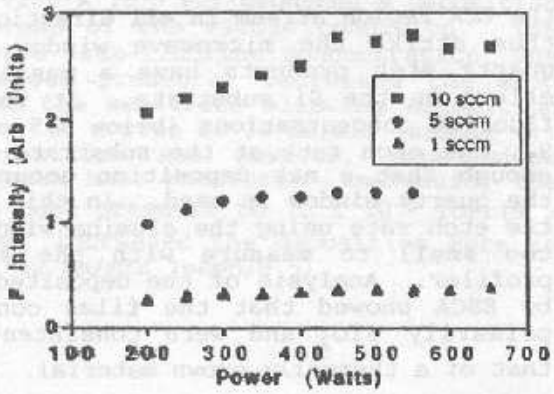

Figure 4. Free fluorine concentration as a function of microwave power for three different etch rates.

ionization becomes significate only at higher electron energies (> 10 eV). These electrons are contained in the tail portion of the Maxwellian distribution. Increasing the microwave power level has an appreciable effect on the concentration of these higher energy electrons. This behavior is seen in the ion current density's dependence on power in Fig. 5. As expected ion current density increases strongly with microwave power due to the increase in the number of high energy electrons. However, current density decreases with SF_6 flow rate. It appears that the higher flow rates deplete the resonance region of lower energy electrons, which suppresses the number which eventual accelerate to higher energies.

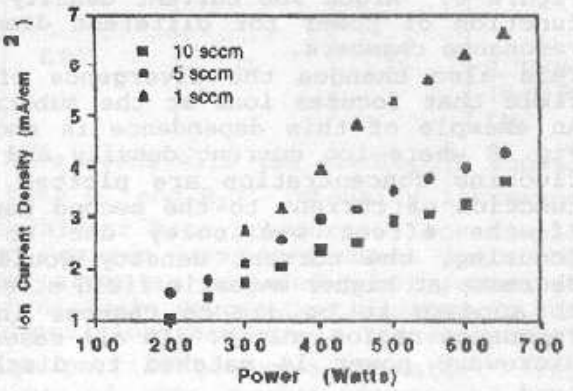

Figure 5. Ion current density as a function of microwave power for three different flow rates.

Decreasing the overall volume of the reactor will assist in reducing gas residence time. The RC diameter was varied by introducing concentric stainless steel inserts which reduced the diameter to 10.2 and 7.8 cm. The effect however, was to reduce ion current density and free fluorine concentration, Figs. 6 and 7. The free fluorine concentration saturated with increasing diameter indicating its effect on it was less than that for ion current density. The reason for the increase could be a larger resonance zone volume, or a decrease in the surface area to volume ratio of the reactor which would reduce wall losses. Another experiment tried was to vary the diameter of the orifice separating the RC from the substrate. The same general behavior was observed. This indicates that the ion portion of the plasma stream remains essential perpendicular to the substrate and the orifice blocks species produced further out in the resonance zone volume from reaching the substrate, which is equivalent to reducing the chamber diameter.

The magnetic field configuration defines the location and shape of the resonance region. This configuration can be modified by moving the magnets or changing the current to the magnets.

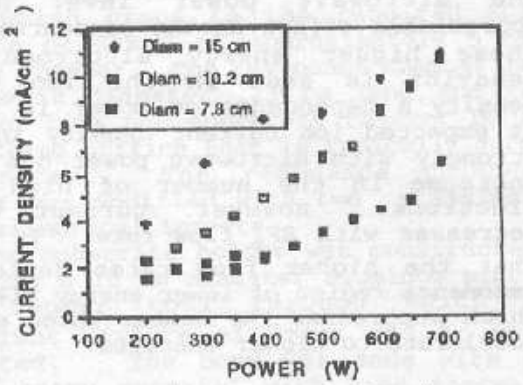

Figure 6. Argon ion current density as a function of power for different diameter resonance chambers.

This also changes the divergence of the field that focuses ions at the substrate. An example of this dependence is show in Fig. 8 where ion current density and free fluorine concentration are plotted as a function of current to the second magnet. If the effect was soley due to ion focusing, the current density would not decrease at higher magnetic field strength. It appears to be due to changes in the resonance region volume. In all cases the microwave power is matched to discharge load.

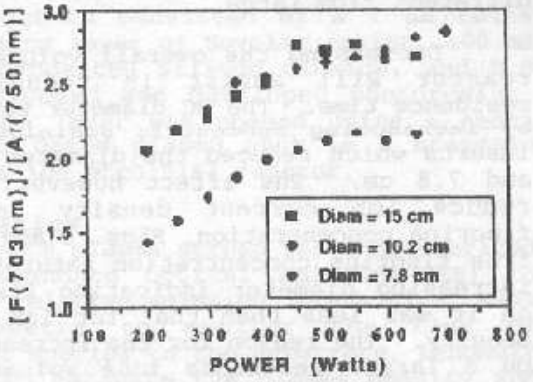

Figure 7. Free fluorine intensity as a function of microwave power for three different resonance chamber diameters.

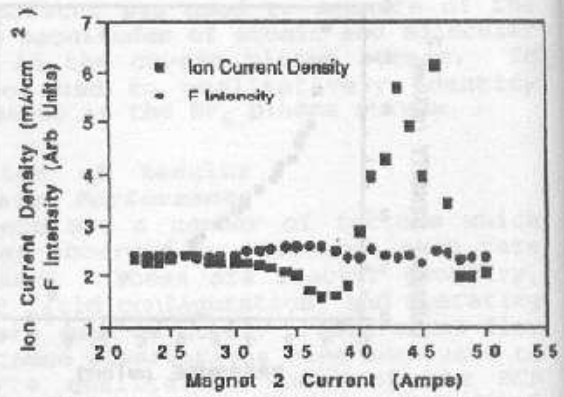

Fig. 8. Ion current density and fluorine concentration as a magnet current.

Composition of Microwave Window:

Microwave power is delivered to the ECR discharge through a dielectric window. The choice of dielectric material is critical because it can impact the plasma and process results. The dielectric material typically used is quartz. In a reactor etching Si with a fluorine plasma, there is a danger of etching the quartz microwave window and redepositing SiO_2 on the substrate. To investigate this possibility, etching studies were performed with the existing system both with and without the addition of a 1 mm thick alumina plate inserted on the vacuum side of the microwave window.

Measured etch rate increases linearly with fluorine concentration until the surface saturates and the reaction becomes surface limited, Fig. 9. The reaction becomes surface limited at about the same fluorine concentration regardless of the microwave window material used. However, the silicon etch rate was lower when the quartz window was used than when the alumina window was in place.

Quartz will etch in a fluorine-containing plasma if subjected to energetic ion bombardment [3-5]. Ions generated in the ECR region stream in all directions and thus strike the microwave window. The quartz etch products have a passivating effect on the Si substrate. At very low fluorine concentrations (below 0.5 on Fig. 9), the etch rate at the substrate is low enough that a net deposition occurs when the quartz window is used. In this range, the etch rate using the alumina window was too small to measure with the surface profiler. Analysis of the deposited films by ESCA showed that the films contained primarily SiO_2 and were consistent with that of a thermally grown material.

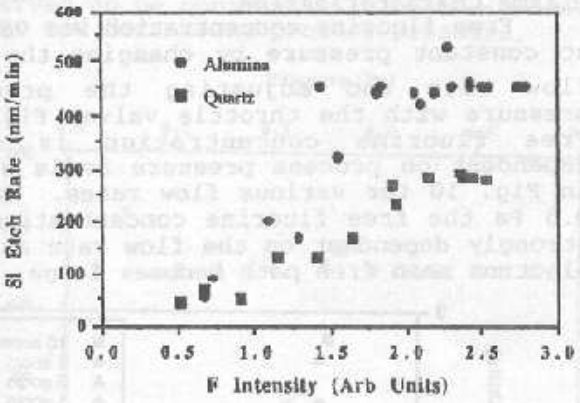

Figure 9. Silicon etch rate as a function of fluorine concentration, with alumina and quartz microwave window.

The fluorine concentration, controlled by varying the SF_6 flow rate, was slightly lower when the quartz window was used due to the loading effect of the quartz. Otherwise the fluorine concentration increased linearly with SF_6 flow rate.

It was found that the SiO_2 deposition rate varied depending on the vacuum condition. Samples 1 and 2 (Table I) were run after an extended pumping time (base pressure 2.0×10^{-5} Torr·(2.7×10^{-3} Pa)). No deposition occurred after either 5 or 10 min process time at 1.0 mTorr(0.13 Pa). This was verified by ESCA where only a native oxide was detected. If, however, as in sample 3, the process is run without an extended pumping time, deposition does occur at a rate of approximately 8 nm/min. The base vacuum was 7×10^{-5} Torr (9×10^{-3} Pa) which contains a substantial partial pressure of water (detected by the quadrupole mass spectrometer).

Reducing the process pressure to 0.5 mTorr (6.5×10^{-2} Pa) produced a deposition regardless of the vacuum condition. The decreased free-fluorine concentration, due to reduced pressure, decreased the etch rate at the substrate allowing deposition to occur at a rate of 20 nm/min (sample 4). The deposition rate, however, depended on the vacuum base pressure. Increasing the vacuum base pressure to $7. \times 10^{-5}$ Torr(9×10^{-3} Pa) increased the deposition rate to almost 40 nm/min (sample 5).

Table 1. Process description of deposited films.

Sample	SF_6 Pressure (Pa)	Thickness Ellipsometer (nm)	Thickness ESCA (nm)	Base Pressure Pa
1	0.13	--	<2	2.7E-03
2	0.13	--	<3	2.7E-03
3	0.13	44	38	9.0E-03
4	0.065	101	98	2.7E-03
5	0.065	192	>100	9.0E-03
6	0.065	32	35	2.7E-03 w/ 1E-02 Pa O_2

Mass scans with the quadrupole showed that both O^+ and H_2O^+ intensity increased at the higher base pressures. For sample 6, dry oxygen was introduced into the reactor after an extended pumping time to see if diatomic oxygen participated in the SiO_2 deposition reaction in the absence of a large partial pressure of water. The addition of dry oxygen decreased the deposition rate to about 6 nm/min. This indicates that water plays a large role in the deposition reaction. The deposition rate decrease with oxygen is expected since adding oxygen to the SF_6 plasma increases the free fluorine concentration [6] as follows:

$$O + SF_n \rightarrow SOF_{n-1} + F \quad (n = 1\text{-}5) \qquad (1)$$

and

$$O + SOF_{n+1} \rightarrow SO_2F_n + F \quad (n = 0\text{-}2). \qquad (2)$$

This increase in fluorine concentration increases the etch rate at the substrate resulting in a decreased net deposition rate.

The plasma stream was analyzed using the quadrupole mass spectrometer with alumina plate covering the quartz window alternately installed. The major differences were the presence of SiF_3^+, SiF_2^+, and SiF^+ and the sulfur-containing species SO^+, SO_2^+, SOF^+, and SOF_2^+ when the quartz window was used. These species were not detected when the alumina window was used.

The principal reaction product, when quartz is etched by SF_6, is SiF_4 [7-9]

which readily fragments to SiF_3^+, SiF_2^+, and SiF^+ in the quadrupole analyzer. The presence of these species when the quartz window was used indicates that the window was etched by the plasma. These are the only silicon-containing species detected and must be the silicon source for the deposition. Considering that water increased the deposition rate, the reaction at the substrate was most likely:

$$3SiF_4 + 2H_2O \rightarrow SiO_2 + 2H_2SiF_6 \quad (3)$$

and fluosilicic acid readily dissociates as follows:

$$H_2SiF_6 \rightarrow SiF_4 + 2HF. \quad (4)$$

These dissociation products are volatile and may have an additional impact on the etch kinetics. HF^+ was not detected and was likely fragmented increasing the fluorine concentration slightly. The sulfur-containing species observed are expected from a SF_6 plasma that has a source of oxygen. Etching the quartz window liberated oxygen, which was taken up by sulfur to form the observed species. This increased the free-fluorine concentration as well (eqs. 1 and 2).

If a quartz microwave window is used, it will be etched and unwanted species will be added to the plasma stream. These species can cause a degradation in process by contaminating the substrate or affecting etch rate. At low fluorine concentrations, SiO_2 redeposits on the substrate in the presence of background water. Care must be taken in the choice of reactor materials to prevent inadvertent process contamination. In an ECR reactor, alumina is the preferred choice for the microwave window when using a fluorine-containing plasma.

Etching Rate Saturation with Fluorine Concentration

A saturation in the Si etch rate is observed for increasing fluorine concentrations, Fig. 9. Previous studies however, have shown that the etch rate of silicon in an SF_6 plasma is directly proportional to the partial pressure of free fluorine[9-12]. These studies indicated that the rate limiting factor is the adsorption fluorine. It is believed that fluorine adsorbs in a multi-layer fashion and it is difficult to saturate the silicon surface with fluorine [13,14]. In this study with an ECR reactor however, experimental data indicates that the etch rate saturates with increasing fluorine concentration. At saturation neither increasing fluorine partial pressure nor increasing ion current density increase the silicon etch rate. However, increasing the ion energy by rf-biasing the substrate does increase the silicon etch rate.

Plasma Characterization

Free fluorine concentration was varied at constant pressure by changing the SF_6 flow rate and adjusting the process pressure with the throttle valve, Fig. 4. Free fluorine concentration is also dependent on process pressure as is shown in Fig. 10 for various flow rates. Below 0.3 Pa the free fluorine concentration is strongly dependent on the flow rate as the electron mean free path becomes large.

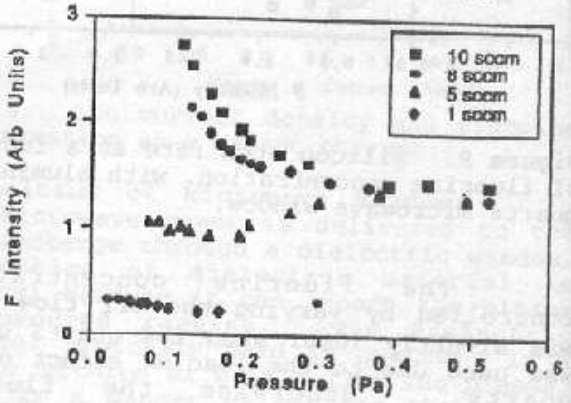

Figure 10. Free fluorine concentration as a function of reactor pressure for four different flow rates.

Ion current density on the other hand is a strong linear function of microwave power and reactor pressure as shown in Fig. 11.

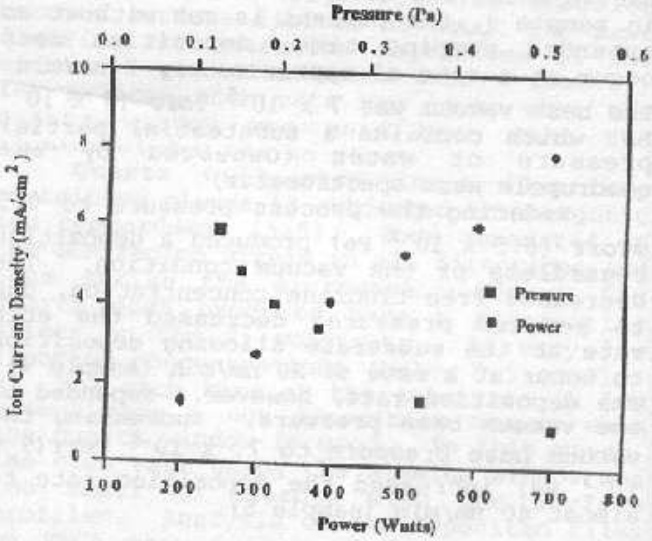

Figure 11. Ion current density as a function of microwave power and reactor pressure.

Silicon Etch Rate

When the fluorine concentration is above saturation, the etch rate was

observed to be constant with both microwave power and decreasing process pressure.

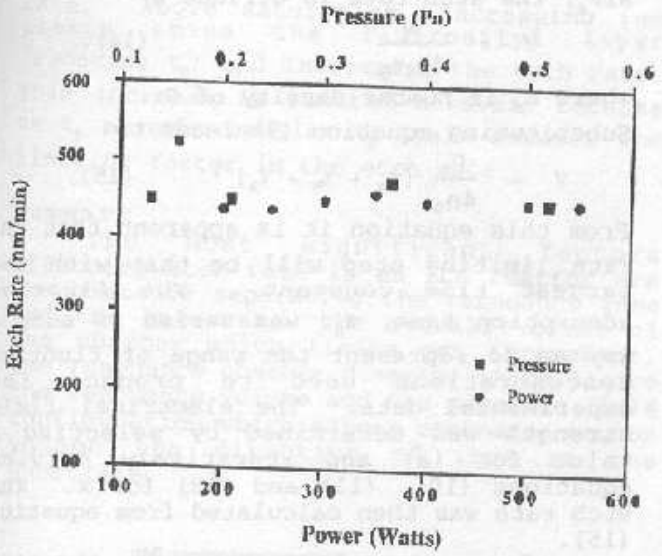

Figure 12. Saturated etch rate as a function of reactor pressure and microwave power.

The ion current density can be varied independently of free fluorine concentration by altering the magnetic field in the resonance chamber. Changing the ion current independent of fluorine concentration had no effect on the silicon etch rate above saturation.

Plasma enhanced etching is viewed as an ion assisted process whose rate has been successfully expressed as:

$$r = j\,\eta\,\sigma_s\,\theta \qquad (5)$$

and the surface coverage is determine from a mass balance on the surface.

$$\theta = \varepsilon\phi/(\eta\sigma_s j + \varepsilon\phi) \qquad (6)$$

The terms are defined as:

r = etch rate
j = ion current density
η = energy coefficient
ε = sticking coefficient
ϕ = free radical flux
σ_s = density of sites.

The ion-induced reaction rate constant, η, is a function of the ion energy. Ion energy can be controlled by rf-biasing the substrate. Silicon etch rate is observed to increase with increasing negative bias, Fig. 13. The etch rate increases with ion energy but not with ion current density or free radical flux. This indicates that equation (5) does not correctly predict the etch rate above saturation.

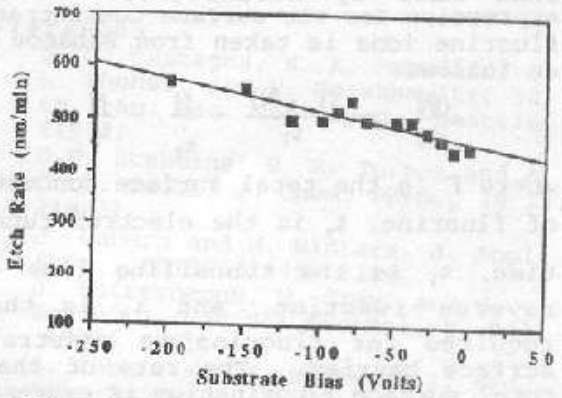

Figure 13. Etch rate as a function of ion energy controlled through RF substrate biasing.

Cabrera-Mott Mechanism

Fluorine spontaneously reacts with silicon to form a thin layer of various silicon fluorides [14-16]. The energy barrier for additional fluorine to penetration this surface is high and some mechanism for lowering the barrier is needed[17-21]. A model based on the Cabrera-Mott mechanism [22] has been developed to explain this barrier lowering and the fluorine etching of silicon [17-21]. The complete solution of this model also predicts a saturation of the silicon etch rate at high free fluorine concentrations and low ion energies. Below saturation the etch rate is limited by the adsorption rate of fluorine.

At saturation the rate is limited by resonant tunnelling of electrons through the insulating fluorinated layer which depends on layer thickness. When a free fluorine atom adsorbs on the fluorinated surface, it abstracts an electron from the silicon bulk due to its high electronegativity. The electron must tunnel from the silicon to the adsorbed fluorine atom. The resultant charge separation produces an electric field across the developing insulating surface layer, this reduces the surface penetration barrier. Continued fluorination of this SiF_x (x = 1,2,3) film produces SiF_4 which is the major volatile etch product.

The field strength, x, across the surface layer is dependent on the surface density of ionized fluorine, N,

$$\xi = \frac{Nq}{\varepsilon_0\,\varepsilon_r} \qquad (7)$$

where q is the electronic charge and ε_0 and ε_r are the vacuum and relative permitivities. In this treatment, ε_r is approximated as 3.9, the relative permittivity of SiO_2. Other assumptions

about the barrier height and location of the absorbed fluorine ion are the same as that made by Babanov[20]. The rate expression for the surface concentration of fluorine ions is taken from Babanov and is as follows:

$$\frac{dN}{dt} = \frac{(\Gamma - N)}{\tau_T} - \frac{N}{\tau_T'} - \frac{N}{\tau_S} \qquad (8)$$

where Γ is the total surface concentration of fluorine, τ_T is the electron tunnelling time, τ_T' is the tunnelling time of the reverse reaction, and τ_S is the time required for fluorine to penetrate the surface barrier. The rate of change of total surface fluorination is expressed as

$$\frac{d\Gamma}{dt} = \frac{(\Gamma_t - \Gamma)}{\tau_A} - \frac{N}{\tau_S} \qquad (9)$$

where Γ_t is the total concentration of adsorption sites on the surface and τ_A is the fluorine adsorption time. If the rate of the reverse tunnelling reaction is assumed to be small, the steady state solution yields

$$N = \frac{\Gamma_t \tau_S}{(\tau_S + \tau_T + \tau_A)} \qquad (10)$$

The mean time for the fluorine ion to penetrate the surface barrier is estimated as

$$\tau_S = \tau_S^o \exp\left\{\frac{(E_s - e\,\xi\,a)}{kT}\right\} \qquad (11)$$

where τ_S^o is estimated by the molecular vibration time (10^{-12} s), E_s is the fluorine penetration barrier height (1.5 eV), and a is the thickness of the fluorosilyl layer. In equation (11), the exponential term is the fraction of fluorine ions energetic enough to overcome the penetration barrier. The electron tunnelling time is estimated by the expression

$$\tau_T = \tau_T^o \exp\left\{\frac{2H}{3\beta}\left[(1+\beta)^{3/2} - 1\right]\right\} \qquad (12)$$

where τ_T^o is estimated by the electron movement frequency (10^{15} s^{-1}) and the exponential factor is the transmission coefficient determined by the WKB approximation [23] where

$$H = \frac{4\pi a(2mV_o)^{1/2}}{h}, \quad \beta = \frac{e\xi a}{V_o}, \qquad (13)$$

and where m is the effective mass of the electron, Vo is the barrier to electron movement, and e is the electronic charge.

Assuming that every fluorine aton that penetrates the surface reacts to form SiF_4, the etch rate is defined by

$$V = \frac{N}{4n_s\tau_S} \qquad (14).$$

where n_s is number density of Si.
Substituting equation (9) leads to

$$V = \frac{\Gamma_t}{4n_s}\left[\tau_S + \tau_T + \tau_A\right]^{-1} \qquad (15).$$

From this equation it is apparent that the rate limiting step will be that with the largest time constant. The fluorine adsorption time, τ_A, was varied in such a way as to represent the range of fluorine concentrations used to produce the experimental data. The electrical field strength was determined by selecting a value for (a) and iteratively solving equations (10), (11) and (12) for x. The etch rate was then calculated from equation (15).

For a given layer thickness the etch rate increases with fluorine concentration and then saturates as shown in Fig. 14. The insert in the figure shows that the saturation etch rate is very sensitive to the fluorosilyl layer thickness.
Below saturation Pelletier's [9,10] assertion that the silicon etch rate is a linear function of fluorine partial pressure still holds. As the fluorine concentration increases, τ_A becomes smaller and τ_T, the resonant tunnelling time, becomes the rate limiting factor. A layer thickness of approximately 1.3 nm predicts an etch rate curve which corresponds to the

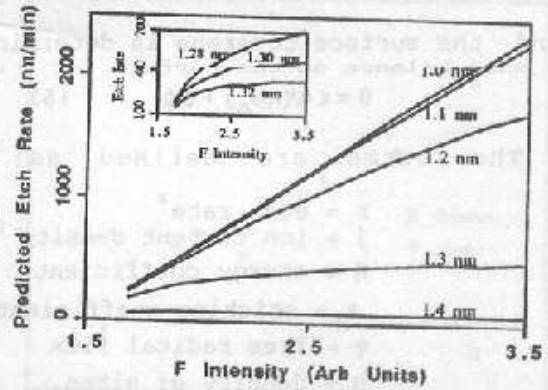

Figure 14. Predicted etch rate as a function of fluorine concentration for several fluorosilyl layer thicknesses.

experimental data obtained in this investigation as shown in Fig. 15. In the range of the variables investigated, τ_S was much less than both τ_A and τ_T and did not limit the etch rate.

The steady state thickness of the SiF_x film is determined by the SiF_4 desorption rate. Above saturation, increasing ion energy thins the fluorosilyl layer (reducing τ_r) and increasing the etch rate. This increase is limited however, because as τ_r becomes smaller τ_h again becomes the limiting factor in the etch rate.

Summary

The most significant factors effecting etch rate in an ECR reactor are the distance separating the resonance zone and the substrate, the overall volume of the chamber which limits gas throughput, the resonance chamber diameter which limits the resonance volume and the magnetic field configuration which alters resonance region volume the direction of ions at the substrate.

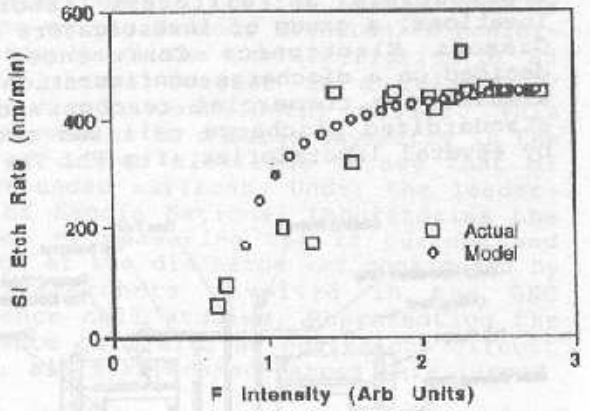

Figure 15. Predicted saturation of the the Si etch rate with fluorine concentration.

Another important consideration is the composition of the microwave window, which in the case of fluorine etching Si, SiO_2 is removed form the window and redeposited on the substrate. This reduces etch rate and conceivably could influence the structure of the etched pattern. An alumina window appears to be a good solution to this particular process problem.

Experimental data shows that silicon etching with SF_6 in an ECR reactor saturates with increasing fluorine concentration. A model based on the Cabrera-Mott mechanism predicts this saturation. The mechanism involves the tunnelling of an electron from the silicon bulk through the SiFx (x=1,2,3) layer to the adsorbed fluorine atoms. At high free fluorine flux, electron tunnelling becomes the rate limiting step producing a saturation. The steady state thickness of the fluorosilyl layer is dependent on ion energy. Increasing ion energy decreases the layer thickness and increases the etch rate.

References

1. T. J. Castagna, K. A. Ashtiani, J. L. Shohet, and N. Hershkowitz, 38 th. Am. Vac. Soc. Symp., Seattle (1992).
2. R.F. Stebbins, B. R. Turner and A. C. H. Smith, J. Chem. Phys., 38 2277 (1963).
3. J. Coburn and H. Winters, J. Appl. Phys., 50(5) (1979) 3189.
4. J. Butterbaugh, D. Gray, and H. Sawin, J. Vac Sci.Technol. B, 9(3) (1991) 1461.
5. J. Coburn and H. Winters, J. Vac. Sci. Technol., 16 (2) (1979) 391.
6. R. d'Agostino and D. Flamm, J. Appl. Phys., 52(1) (1981) 162.
7. A. Picard, G. Turban, and B. Grolleau, J. Phys. D: Appl. Phys., 19 (1986) 991.
8. D. Flamm, V. Donnelly, and J. Mucha, J. Appl. Phys., 52 (5) (1981) 3633.
9. J. Pelletier and M. Cooke, J. Vac. Sci. Technol. B, 7 (1), 59 (1989).
10. B. Petit and J. Pelletier, Jpn. J. Appl. Phys., 26 (6), 825 (1987).
11. K. Ninomiya, K. Suzuki, S. Nishimatsu, and O. Okada, J. Appl. Phys., 58(3), 1177 (1985).
12. J. Pelletier, Appl Phys. Lett., 53(17), 1665 (1988).
13. J. Pelletier, J. Phys. D, 20, 858 (1987).
14. C. Stinespring and A. Freedman, Appl. Phys. Lett., 48(11), 718 (1986).
15. M. Seel and P. Bagus, Phys. Rev. B, 28(4), 2023 (1983).
16. F. McFeely, J. Vac. Sci. Technol. A, 3(3), 879 (1985).
17. H. Winters, J. Coburn, and T. Chuang, J. Vac. Sci. Technol. B, 1(2), 469 (1983).
18. C. Van de Walle, F. McFeely, and S. Pantelides, Mater. Sci. Forum, 38-41, 335 (1989).
19. Y. Babanov, A. Prokaznikov, and V. Svetovoy, J. Phys. Condens. Matter, 1, SB197 (1989).
20. Y. Babanov, A. Prokaznikov, and V. Svetovoy, Vacuum, 41 (4-6), 902 (1990).
21. F. Houle, Phys. Rev. B, 39(14), 10120 (1989).
22. N. Cabrera and N. Mott, Rep. Prog. Phys., 12, 163 (1949).
23. A. Fromholt, Quantum Mechanics for Applied Physics and Engineering, Academic Press, New York, p. 244 (1981).